Preferential Occurrence of Fast Radio Bursts in Massive Star-Forming Galaxies

Kritti Sharma[1,*], Vikram Ravi[1,2], Liam Connor[1], Casey Law[1,2], Stella Koch Ocker[1,3], Myles Sherman[1], Nikita Kosogorov[1,2], Jakob Faber[1,], Gregg Hallinan[1,2], Charlie Harnach[1,2], Greg Hellbourg[1,2], Rick Hobbs[1,2], David Hodge[1,2], Mark Hodges[1,2], James Lamb[1,2], Paul Rasmussen[1,2], Jean Somalwar[1], Sander Weinreb[1], David Woody[1,2], Joel Leja[4,5,6], Shreya Anand[1], Kaustav Kashyap Das[1], Yu-Jing Qin[1], Sam Rose[1], Dillon Z. Dong[1,7], Jessie Miller[1], Yuhan Yao[1,8]

[1]*Cahill Center for Astronomy and Astrophysics, MC 249-17 California Institute of Technology, Pasadena, CA 91125, USA.*

[2]*Owens Valley Radio Observatory, California Institute of Technology, Big Pine, CA 93513, USA.*

[3]*The Observatories of the Carnegie Institution for Science, Pasadena, CA 91101, USA.*

[4]*Department of Astronomy & Astrophysics, The Pennsylvania State University, University Park, PA 16802, USA.*

[5]*Institute for Computational & Data Sciences, The Pennsylvania State University, University Park, PA, USA.*

[6]*Institute for Gravitation & the Cosmos, The Pennsylvania State University, University Park, PA 16802, USA.*

[7]*National Radio Astronomy Observatory, 1003 Lopezville Road, Socorro, NM, 87801, USA.*

[8]*Department of Astronomy, University of California, Berkeley, CA 94720-3411, USA.*

[*]*Correspondence email: kritti@caltech.edu*

Fast Radio Bursts (FRBs) are millisecond-duration events detected from beyond the Milky Way. FRB emission characteristics favor highly magnetized neutron stars, or magnetars, as the sources[1], as evidenced by FRB-like bursts from a galactic magnetar[2,3], and the star-forming nature of FRB host galaxies[4,5]. However, the processes that produce FRB sources remain unknown[6]. Although galactic magnetars are often linked to core-collapse supernovae (CCSNe)[7], it's uncertain what determines which supernovae result in magnetars. The galactic environments of FRB sources can be harnessed to probe their progenitors. Here, we present the stellar population properties of 30 FRB host galaxies discovered by the Deep Synoptic Array. Our analysis shows a significant deficit of low-mass FRB hosts compared to the occurrence of star-formation in the universe, implying that FRBs are a biased tracer of star-formation, preferentially selecting massive star-forming galaxies. This bias may be driven by galaxy metallicity, which is positively correlated with stellar mass[8]. Metal-rich environments may favor the formation of magnetar progenitors through stellar mergers[9,10], as higher metallicity stars are less compact and more likely to fill their Roche lobes, leading to unstable mass transfer. Although massive stars do not have convective

interiors to generate strong magnetic fields by dynamo[11], merger remnants are thought to have the requisite internal magnetic-field strengths to result in magnetars[11,12]. The preferential occurrence of FRBs in massive star-forming galaxies suggests that CCSN of merger remnants preferentially forms magnetars.

The Deep Synoptic Array (DSA-110), situated at the Owens Valley Radio Observatory (OVRO) near Bishop, California, is a radio interferometer built for simultaneous FRB discovery and arcsecond -scale localization. The DSA-110 underwent science commissioning and performed observations between February 2022 and March 2024 with a coherent core of 48 4.65 m antennas used for FRB searching combined with 15 outrigger antennas (maximum baseline of 2.5 km) used for localization. Each antenna is equipped with a dual-polarization ambient-temperature 1.28–1.53 GHz receiver. A custom low-noise amplifier design delivering 7 K noise temperature[13] was central to achieving sensitivity to 1.9 Jy ms FRBs (for millisecond-duration events). A real-time search for FRBs with 0.262 ms sampling and a dispersion-measure (DM) range up to 1500 pc cm^{-3} was conducted. Localization accuracies of better than $\pm$2 arcsecond (90% confidence) were achieved by comparison with coeval observations of standard astrometric reference sources (see Methods and Supplementary Fig. 1, 2). During these observations, 60 FRBs were successfully localized.

In this work, we limit our analysis to FRBs discovered up to November 2023 which have redshifts for all hosts detectable down to r = 23.5 mag, to ensure a uniform sample selection. The follow-up of a subset of FRBs discovered post November 2023 is presented in our companion paper (Connor et al.). Among the 42 FRBs localized by DSA-110 up to November 2023, 30 had a potential host-galaxy candidate in the vicinity of the FRB localization (within 10″), detectable at $\leq$ 23.5 mag in archival r-band data from PanSTARRS1 (PS1)[14] or the Beijing-Arizona Sky Survey (BASS) from the Dark Energy Survey[15]. We complement these archival data with deeper ground-based optical or near-infrared imaging observations with the Wafer-Scale Imager for Prime focus (WaSP)[16] and the Wide Field Infrared Camera (WIRC)[17] instruments, mounted on the 200-inch Hale Telescope at the Palomar Observatory in our follow-up campaigns (see Methods). We use the Bayesian Probabilistic Association of Transients to their Hosts (PATH) formalism[18] on the deepest available imaging data to estimate the association probability (P_{host}) of the most likely host galaxy (see Methods). The PATH analysis finds secure host associations for 26 FRBs with $P_{host} \geq 90\%$ (see Extended Data Fig. 1). Of the remaining four events, FRBs 20221027A and 20220330D have two possible hosts, one of which is favored by both the localizations and the DMs (see Methods). FRB 20230216A is found at a large offset from the preferred host, which lowers the association probability according to the chosen PATH setup, and the localization of FRB 20220208A is confused by the presence of a faint (23.4 mag in J-band data, spectroscopic redshift not available) alternative host. We further validate our host associations in Methods and Supplementary Fig. 3, 4. We also discuss the hostless FRBs in Methods and Supplementary Fig. 5. The imaging mosaic of 30 FRB hosts included in our sample is displayed in Fig. 1 (see

Supplementary Fig. 6 for labeled axes), and the discovery properties of the host galaxies are tabulated in Extended Data Table 1. For all quantitative arguments in our work, we only consider secure host associations with $P_{host} \geq 90\%$.

Having identified the most probable host galaxies, we obtained optical spectroscopy with the Low Resolution Imaging Spectrometer (LRIS)[19] on Keck-I, DEep Imaging Multi-Object Spectrograph (DEIMOS)[20] on Keck-II at W. M. Keck Observatory and the Double Spectrograph (DBSP)[21] on the 200-inch Hale Telescope at Palomar Observatory (see Methods). The spectroscopic redshifts (z) and emission line fluxes are measured by jointly fitting the stellar continuum and nebular emission using the penalized PiXel-Fitting (`pPXF`) software[22] (see Supplementary Fig. 7 and Table 1). Next, we model the spectral energy distributions (SEDs) of the FRB host galaxies using the `Prospector` software[23], where we jointly forward model the observed spectra, archival photometry from PS1, BASS, Mayall z-band Legacy Survey (MzLS)[24], Sloan Digital Sky Survey (SDSS)[25], Two Micron All Sky Survey (2MASS)[26], Wide-field Infrared Survey Explorer (WISE)[27], and Galaxy Evolution Explorer (GALEX)[28] surveys and photometry of data obtained with WaSP and WIRC instruments (see Supplementary Table 2). We model the galaxies with a seven-component non-parametric star-formation history (SFH), a two-component dust attenuation model, a flexible dust attenuation curve, dust emission, and a self-consistent nebular emission model (see Methods and Supplementary Table 3 for a summary of model parameters). Using standard empirical optical emission-line diagnostic diagrams[29,30] (see Extended Data Fig. 2) and WISE color-color galaxy classifications[31] (see Extended Data Fig. 3), we find that the dominant ionization mechanism in FRB host galaxies is consistent with the locus of star-forming galaxies (late-type spirals) and emission line galaxies with active galactic nuclei (AGN, either LINERs or Seyferts) (see Methods and Supplementary Table 4). Therefore, we also include the emission from dust-enshrouded AGN in our SED modeling. The derived properties from our SED fits (see Supplementary Fig. 8) and constrained SFHs (see Supplementary Fig. 9) for FRB host galaxies are tabulated in Extended Data Table 2, and their distributions are shown in Extended Data Fig. 4.

To contextualize FRB host galaxies within the broader framework of star-formation and stellar mass in the universe, we compare them with the background galaxy population. In our comparison sample, alongside our 26 secure host associations, we include a complete literature sample of 26 FRB hosts[4,5] that adhere to our selection criteria of r-band magnitude $\leq$ 23.5 mag and secure host association ($P_{host} \geq 90\%$). To address incompleteness inherent in magnitude-limited galaxy surveys, we adopted a hybrid approach to simulate the complete background galaxy population. We sample the galaxy stellar masses, M_*, from the stellar mass function, $\Phi(M_*, z)$[32] and then compute the corresponding star-formation rate (SFR) using the star-forming main sequence, $SFR(M_*, z)$[33] and the distribution of galaxies in $\log M_* - \log SFR - z$ space[33] (see Methods and Supplementary Fig. 10, 11). We compare the stellar mass distribution of FRB hosts with the distributions of stellar mass of background galaxies selected by two methods – weighted by SFR and weighted by stellar mass. We split the FRB comparison sample into three redshift bins to mitigate biases from the evolution of the background galaxy population: $z \leq 0.2$ with 20 FRBs, $0.2 < z \leq 0.4$ with 24 FRBs, and $0.4 < z \leq 0.7$ with 7 FRBs. The lowest redshift bin edge was chosen based on our capability to confidently identify low mass galaxies, given the optical imaging depths (see Methods). Notably, FRB 20221029A was excluded from this analysis due to its solitary occurrence at $z \sim 1$, rendering meaningful comparisons challenging at high redshifts owing to limited statistical power. We perform one-sample Kolmogorov-Smirnov (KS) tests between the sample of FRB stellar masses, and the background distributions corrected for optical selection effect of r-band magnitude ≤ 23.5 mag (see Methods). The results are shown in Fig. 2.

We find that the sample of FRB host-galaxy stellar masses is inconsistent with the stellar mass distribution in the universe, but broadly consistent with the distribution of galaxies selected according to SFR. In all three redshift bins, the KS-test p-value from the comparison between FRBs and galaxies selected according to stellar mass is < 0.001 (i.e., $> 3\sigma$ significance). Conversely, the comparison with the stellar mass distribution of galaxies selected according to SFR yields p-values greater than 0.01 in all the three redshift bins. This similarity to galaxies selected by SFR is further emphasized by the close alignment of FRB host galaxies with the star-forming main sequence of galaxies[4,34] (see Extended Data Fig. 5). However, for $z \leq 0.2$, despite our sensitivity to optically faint galaxies, we observe a notable scarcity of FRBs in the galaxies with $\log M_* \lesssim 9$ (see Fig. 2a). This is indicated by the low associated KS-test result of p = 0.030; we note that the KS-test is not optimal to quantify the significance of this claim. Radio selection effects are not expected to contribute to this scarcity of low-mass FRB hosts at $z \leq 0.2$[35] (see Methods).

The dearth of $z \leq 0.2$ low-mass FRB host galaxies becomes even clearer when we compare them to host galaxies of the most prevalent class of CCSNe (Type II), which trace the occurrence of star-formation in the universe, with no dependence on other galaxy properties[36] (see Fig. 3b). We show the distribution of stellar masses of Type II CCSNe and FRB host galaxies in the r-band magnitude and redshift space in Fig. 3a. FRB hosts trace the locus of $0.1 - 1\ L_*$ background galaxies, and are more massive than typical Type II CCSNe host galaxies. To contextualize the rarity of the occurrence of Type II CCSNe in only massive galaxies on the scale of our $z \leq 0.2$ FRB sample size (N_{FRB}), we perform 1,000 Monte-Carlo simulations where we sample N_{FRB} galaxy stellar masses from the Type II CCSNe host distributions. We compute the fraction of these samples with all stellar masses above a particular stellar mass $\log M_*$ (see Extended Data Fig. 6). We find that for our complete local universe FRB sample of size $N_{FRB} = 20$, the probability that all Type II CCSNe occur in galaxies more massive than $10^9\ M_\odot$ is p = 0.0014 ($\sim 3.2\sigma$ significance). If FRBs were an unbiased tracer of star-formation in the universe, then this quantifies the significance of the deficit of low-mass FRB hosts.

We have shown that FRBs trace the occurrence of star-formation in the universe in preferentially massive galaxies. This could point to an environment-dependent production efficiency of FRB sources. The primary driver of changes in stellar population properties with galaxy mass is the galaxy mass-metallicity relation[8]. Increased metallicity affects the evolution of massive stars by line-driven stellar winds, where the mass-loss rate positively correlates with metallicity. Certain classes of supernova preferentially occur in low-metallicity environments[37], such as those that produce long-duration gamma-ray bursts (lGRBs) and superluminous supernovae (SLSNe)[36]. We quantify the effect of metallicity on the selection of FRB host galaxies by constructing background stellar mass distributions weighted by SFR together with a metallicity-dependent FRB source formation efficiency $\rho = (1 + (-M/M_c)^{\beta})^{-1}$. Here, M_c is a characteristic cut-off mass that regulates the production of FRB sources, ceasing their occurrence in lower stellar mass (and hence, lower metallicity) galaxies and β regulates the strength of the metallicity cutoff. The best-fitting model suggests a strong cutoff with $\log M_c = 8.86$ (see Fig. 3b), thus implying that the formation efficiency of FRB sources is suppressed at oxygen abundances below $12 + \log \mathrm{O/H} \sim 8.09^{+0.60}_{-0.51}$, corresponding to a cutoff metallicity of $\log(Z/Z_\odot) = -0.60^{+0.60}_{-0.51}$. We determine this threshold metallicity by employing the galaxy mass-metallicity relation[8], which is incorporated as a prior in our SED modeling methodology (see Methods).

We have interpreted the preferential occurrence of FRBs in massive star-forming galaxies as a preference for high metallicity environments, as inferred from the positive correlation between galaxy stellar mass and metallicity[8]. Magnetars are known to be potential FRB sources[1] and the preferential occurrence of FRBs in higher metallicity environments may be expected in the scenario[1] that FRBs are emitted by magnetars formed in a sub-population of CCSNe. First, for single-star progenitors, elevated metallicity would favor the formation of neutron star remnants over black holes due to increased mass-loss in higher metallicity stars[38]. Further, stellar mergers have been theoretically demonstrated as the origin of magnetic blue straggler stars, which undergo rejuvenation by burning the accreted fuel from their companions, and are believed to be potential progenitors of magnetars due to the amplified magnetic fields of the merger remnants[12]. The increase in the metallicity of intermediate-mass progenitor stars evolving in such binaries, which eventually culminate in CCSNe, increases the proportion of CCSNe occurring through this delayed binary evolution channel[9,10]. The heightened efficiency of CCSN formation through binary interactions in high-metallicity settings likely stems from the association between metallicity and stellar size[10]. A star with higher metallicity is less compact as it evolves beyond the main sequence, thereby affecting the progression of mass transfer in binary systems[39]. At high metallicity, stars in binaries are more likely to evolve to fill their Roche lobes, leading to unstable mass transfer and stellar mergers that potentially produce magnetar progenitors. A stellar-merger formation channel for magnetar progenitors may indeed be observationally favored for the Galactic magnetar population[40].

We broaden our understanding of FRB sources by comparing the distributions of host-normalized projected galactocentric offsets and host galaxy stellar mass with various classes of transients (see Fig. 4 and Methods for a description of the literature samples used). We limit our comparisons to the local universe ($z \leq 0.2$) to potentially mitigate any unknown incompleteness that might be inherent to other transients at high redshifts. We also show the distribution for the entire redshift range in Extended Data Fig. 7 and 8. We correct the galaxy stellar mass distributions for the redshift evolution and perform two-sample KS-tests to quantify the potential similarities (see Methods and Supplementary Table 5). In contrast to FRBs, the SLSNe and lGRBs predominantly manifest in the central star-forming regions of low-mass galaxies characterized by low metallicity and high specific SFR, thus underscoring the dissimilarities with FRBs. Although the offset distribution of ultra-luminous X-ray (ULX) sources is consistent with FRBs ($p_{KS} = 0.09$), they demonstrate a preference for occurrence in massive galaxies and trace the background galaxy population selected by stellar mass, not star-formation. The stellar mass distribution of FRB host galaxies is comparable to those of other classes of transient that trace star-formation, including Type II CCSNe, Type Ia supernovae, and short-duration GRBs (sGRBs), but with the deficit of low-mass galaxies.

Some differences are apparent in the offset distributions of FRBs and classes of transients that trace star formation. Although FRBs are systematically found at larger offsets than Type II CCSNe and Type Ia supernovae, but smaller offsets than sGRBs, the host-normalized offsets are consistent with these three transient classes, owing to massive FRB host galaxies and the positive galaxy stellar mass - radius correlation. The larger absolute offset values may be a consequence of the radio-observation bias, where bursts originating closer to the center of star-forming spiral galaxies are over-dispersed and exhibit higher scattering timescales[35], thus preventing their detection. If FRBs were to trace the locations of star-formation within their host galaxies, this radio selection bias may shift the FRB offset distribution to lower offsets by up to ~ 1 kpc[41]. On the other hand, the larger FRB offsets may be indicative of the long delays in CCSNe involving interacting binaries, which would imply that the CCSNe occur significantly displaced from the birth sites[9]. For example, if the typical stellar motions at the birth site are ~ 10 km s^{-1} and the delay-time is 75 Myr, then the system would have drifted by 750 pc before the explosion. Alternatively, the larger offsets of FRBs may also arise from the contribution of non-CCSNe formation channels, such as the accretion- or merger-induced collapse (AIC/MIC) of massive white dwarfs and binary neutron star mergers, towards FRB sources. The existence of these FRB source formation channels is indicated by the globular cluster FRB source 20201120E[42,43], and early DSA-110 results[34]. To conclude, the larger offsets of FRBs may either be due to delayed pre-CCSNe stellar merger magnetar formation scenario, or due to contributions from non-CCSN formation channels. However, we note that the current data shows no evidence for the existence of multiple statistically different FRB host galaxy populations (see Methods).

Further insight into source formation channels may be gained through a detailed analysis of the distribution of FRB delay-times with respect to the formation of their stellar progenitors[44]. Non-CCSN channels (e.g., AIC/MIC of white dwarfs) are expected to have extended delay-time distributions of several Gyr[45], whereas CCSNe of isolated stars occur on $\sim 3-50$ Myr stellar lifetimes, and the CCSNe of stellar-merger remnants are expected to occur promptly within $\sim 50-250$ Myr of the birth of binary components[9]. The preferential occurrence of FRBs in massive star-forming galaxies is a constraint that applies to any model for FRB source formation. The influence of metallicity on the formation of FRB sources can be independently corroborated using forthcoming surveys. Given that star-formation in the early universe predominantly occurs within low-mass galaxies, and galaxies of the same stellar mass at higher redshifts are less chemically enriched[46], the preference of FRBs for metal-rich environments implies a suppression of the proposed FRB source formation channel at high redshifts. However, scenarios proposed for the repeating FRB 121102[47], which is found in a low-metallicity dwarf star-forming galaxy, may become more common at high redshifts. If most FRBs are emitted by magnetars like those observed in the Milky Way, our results favor a scenario where magnetars are generally formed from the CCSN of stellar merger remnants in interacting binaries.

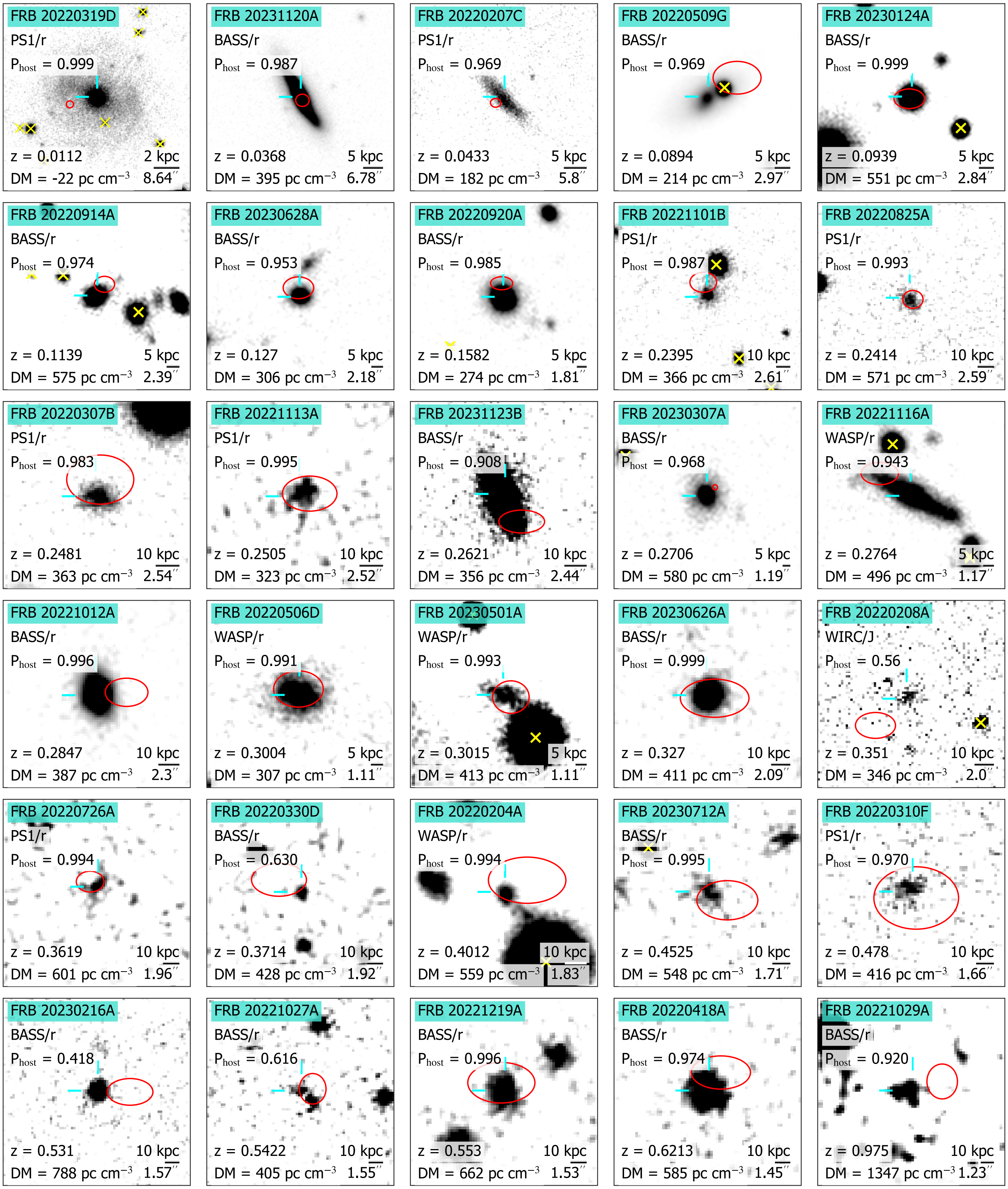

Fig.1: Optical/IR imaging of the fields of DSA-110 discovered FRBs. The images are centered on the PATH-identified host galaxies (cyan crosshairs), and panels are arranged in increasing order of redshifts (see Extended Data Table 1). The 90% confidence FRB localization regions are marked as red ellipses and stars are marked as yellow crosses. These images reach 3σ depths of $\gtrsim 23-24$ mag and are oriented with north up and east to the left. The imaging instrument, association probability, extragalactic DM, redshift, and physical scales are marked on the panels for reference. All images were smoothed with a Gaussian kernel of $\sigma = 0''.15$ to improve visibility.

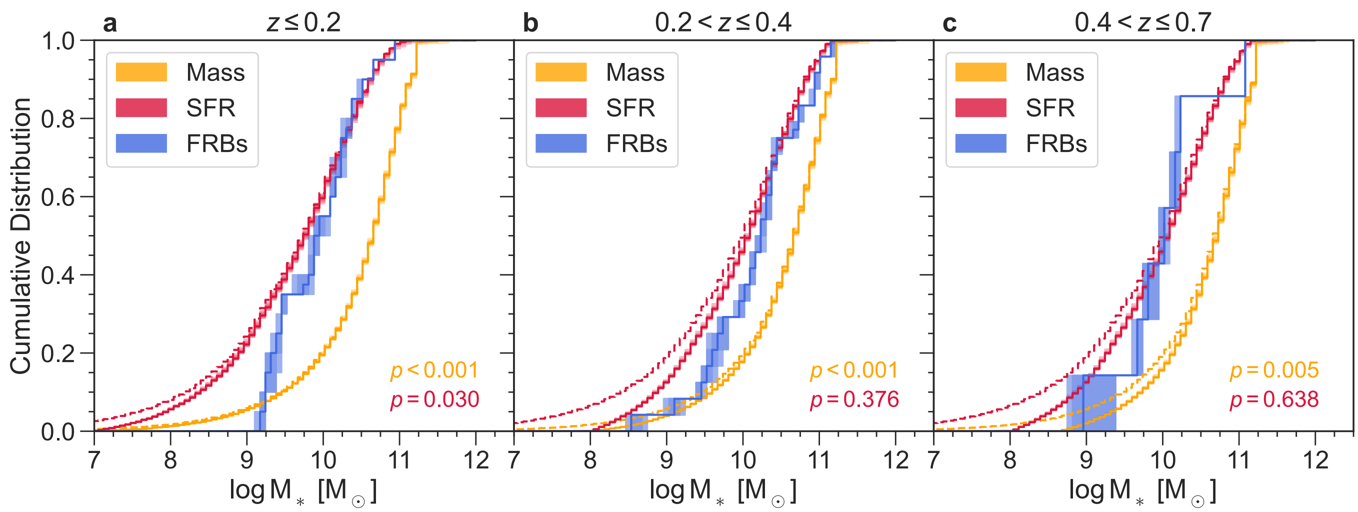

Fig.2: Comparison of FRB host galaxies with the distribution of galaxies in the Universe selected by stellar mass and star-formation. We show cumulative distributions of galaxy stellar mass of samples selected in three ways: the occurrence of FRBs (blue), SFR (red), and stellar mass (orange). We correct the background stellar mass distributions for optical selection effects by employing an r-band magnitude threshold of 23.5 mag (solid lines, see Methods). For reference, we also plot the distributions without this selection (dashed lines). The shaded regions represent the $1, 2, 3\sigma$ bands. Along with 26 secure host associations of DSA-110 FRBs from this work, we also include the Gordon et al.[4] and Bhardwaj et al.[5] sample of FRB host galaxies that follow our selection criterion. The distribution of FRB-host stellar masses is inconsistent with the distribution of background galaxies selected by stellar mass in all redshift bins with $> 3\sigma$ confidence. The p-value computed using the KS-test for similarity with the distribution of background galaxies selected by SFR (red) is $\gtrsim 0.01$ in all redshift bins, indicating that the occurrence of FRBs is correlated with the occurrence of star-formation. However, despite our sensitivity, there is a deficit of low-mass FRB hosts in $z \leq 0.2$ bin.

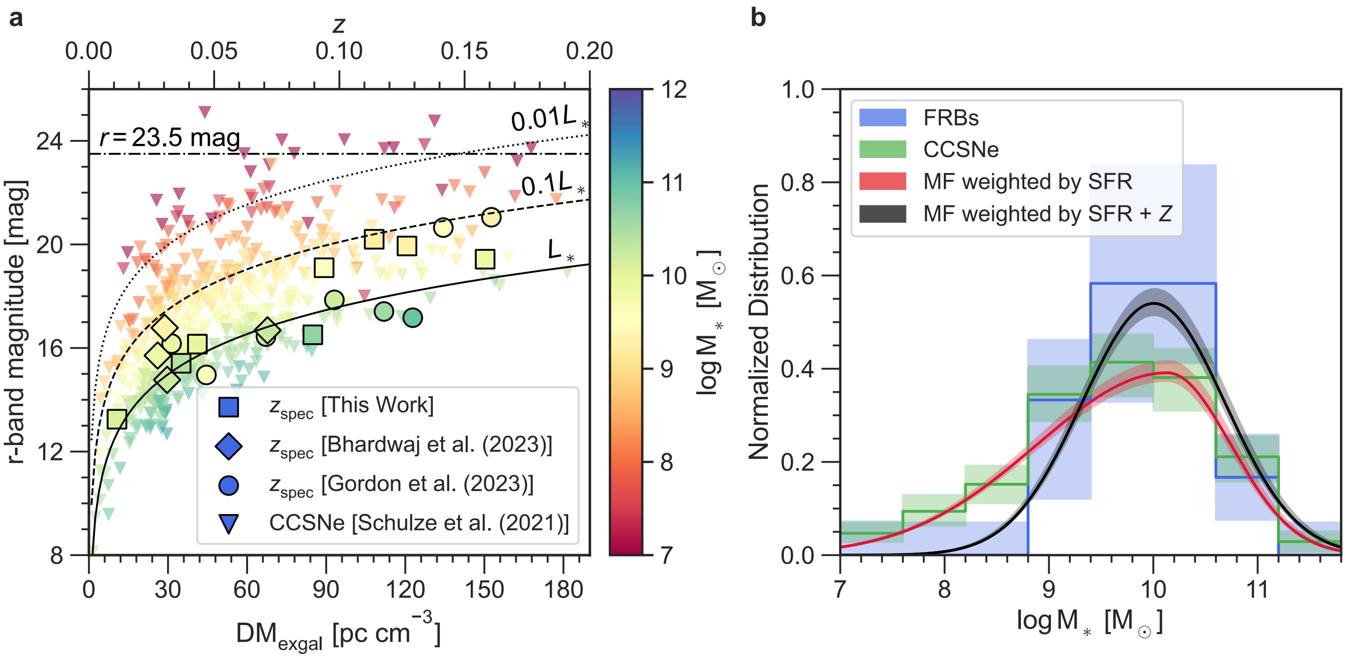

Fig.3: Investigation of whether FRBs trace star-formation in the universe using the $z \leq 0.2$ **sample.** The panel **a** shows the distribution of the r-band magnitude and redshift of FRB hosts published in this work (squares), alongside Gordon et al.[4] (circles) and Bhardwaj et al.[5] (diamonds) FRB host galaxies samples with r-band magnitude $\lesssim$ 23.5 mag (dashdot line) and $z \leq 0.2$. On comparing with the redshift evolution of galaxies with characteristic luminosities L_* (solid line), $0.1L_*$ (dashed line), and $0.01L_*$ (dotted line) , we find that the FRB hosts trace ~ 0.1–$1L_*$ galaxies. A comparison with the host galaxies of Type II CCSNe[36] (triangles) reveals that FRB host galaxies are relatively massive. This result is also evident in panel **b**, where we show the host galaxy mass distributions (solid lines) with Poisson errors (shaded regions). Since Type II CCSNe (green) are unbiased tracers of star-formation in the universe, the SFR-weighted galaxy mass distribution (red) provides an adequate description of their host mass distribution. On the other hand, the host galaxies of FRBs (blue) show a clear dearth of low-mass galaxies. This absence can be accounted for by adding a metallicity-dependent FRB progenitor formation efficiency (black), which is stifled in environments with oxygen abundances, 12+log(O/H) $\leq 8.09^{+0.60}_{-0.51}$, corresponding to a cutoff metallicity of $\log(Z/Z_\odot) = -0.60^{+0.60}_{-0.51}$.

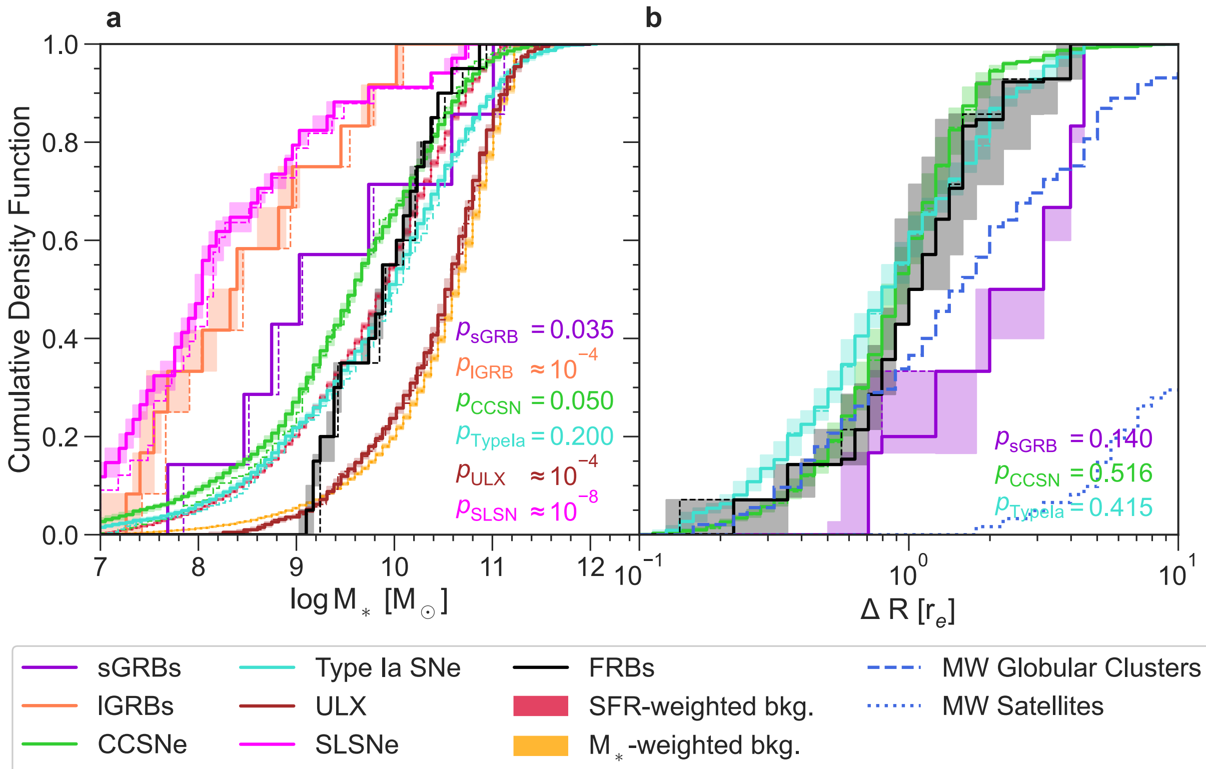

Fig.4: Comparison of FRB host galaxy properties with those of various transient classes at $z \leq 0.2$**.** We compare host galaxy stellar mass (panel **a**) and host-normalized galactocentric offset (panel **b**) distributions of FRBs with Type Ia supernovae , ultra-luminous X-ray sources (ULX) , superluminous supernovae (SLSNe) , core-collapse supernovae (CCSNe) , short-duration gamma ray bursts (sGRBs) and long-duration gamma ray bursts (lGRBs) (see Methods for a description of the comparison samples). For comparisons, we only use our secure FRB host associations, together with the literature sample of FRB host galaxies and offset measurements (see Methods). We correct stellar masses for redshift evolution[41] (see Methods). The measured values (dashed lines), median (thick lines) and 1σ errors (shaded regions) computed using 1,000 Monte Carlo samples of measurements reported in literature are plotted. For reference, we also plot the background population selected by stellar mass (orange) and SFR (red) in panel **a** (see Fig. 2) and offsets of the satellites and globular clusters of Milky Way (MW) in panel **b**.

References

[1] Zhang, B. The physics of fast radio bursts. *Reviews of Modern Physics* **95**, 035005, DOI: https://dx.doi.org/10.1103/RevModPhys.95.035005 (2023). 2212.03972.

[2] CHIME/FRB Collaboration et al. A bright millisecond-duration radio burst from a Galactic magnetar. *Nature* **587**, 54–58, DOI: https://dx.doi.org/10.1038/s41586-020-2863-y (2020). 2005.10324.

[3] Bochenek, C. D. et al. A fast radio burst associated with a Galactic magnetar. *Nature* **587**, 59–62, DOI: https://dx.doi.org/10.1038/s41586-020-2872-x (2020). 2005.10828.

[4] Gordon, A. C. et al. The Demographics, Stellar Populations, and Star Formation Histories of Fast Radio Burst Host Galaxies: Implications for the Progenitors. *The Astrophysical Journal* **954**, 80, DOI: https://dx.doi.org/10.3847/1538-4357/ace5aa (2023). 2302.05465.

[5] Bhardwaj, M. et al. Host Galaxies for Four Nearby CHIME/FRB Sources and the Local Universe FRB Host Galaxy Population. *arXiv e-prints* arXiv:2310.10018, DOI: https://dx.doi.org/10.48550/arXiv.2310.10018 (2023). 2310.10018.

[6] Popov, S. B. High magnetic field neutron stars and magnetars in binary systems. In Troja, E. & Baring, M. G. (eds.) Neutron Star Astrophysics at the Crossroads: Magnetars and the Multimessenger Revolution, vol. 363, 61–71, DOI: https://dx.doi.org/10.1017/S1743921322000308 (2023). 2201.07507.

[7] Kaspi, V. M. & Beloborodov, A. M. Magnetars. *Annual Review of Astron and Astrophys* **55**, 261–301, DOI: https://dx.doi.org/10.1146/annurev-astro-081915-023329 (2017). 1703.00068.

[8] Gallazzi, A., Charlot, S., Brinchmann, J., White, S. D. M. & Tremonti, C. A. The ages and metallicities of galaxies in the local universe. *Monthly Notices of the Royal Astronomical Society* **362**, 41–58, DOI: https://dx.doi.org/10.1111/j.1365-2966.2005.09321.x (2005). astro-ph/0506539.

[9] Zapartas, E. et al. Delay-time distribution of core-collapse supernovae with late events resulting from binary interaction. *Astronomy and Astrophysics* **601**, A29, DOI: https://dx.doi.org/10.1051/0004-6361/201629685 (2017). 1701.07032.

[10] Zapartas, E. et al. The diverse lives of progenitors of hydrogen-rich core-collapse supernovae: the role of binary interaction. *Astronomy and Astrophysics* **631**, A5, DOI: https://dx.doi.org/10.1051/0004-6361/201935854 (2019). 1907.06687.

[11] Frost, A. J. et al. A magnetic massive star has experienced a stellar merger. *Science* **384**, 214–217, DOI: https://dx.doi.org/10.1126/science.adg7700 (2024). 2404.10167.

[12] Schneider, F. R. N. et al. Stellar mergers as the origin of magnetic massive stars. *Nature* **574**, 211–214, DOI: https://dx.doi.org/10.1038/s41586-019-1621-5 (2019). 1910.14058.

[13] Weinreb, S. & Shi, J. Low Noise Amplifier With 7-K Noise at 1.4 GHz and 25 ℃. *IEEE Transactions on Microwave Theory Techniques* **69**, 2345–2351, DOI: https://dx.doi.org/10.1109/TMTT.2021.3061459 (2021).

[14] Chambers, K. C. et al. The Pan-STARRS1 Surveys. *arXiv e-prints* arXiv:1612.05560 (2016). 1612.05560.

[15] Zou, H. et al. Project Overview of the Beijing-Arizona Sky Survey. *Publications of the ASP* **129**, 064101, DOI: https://dx.doi.org/10.1088/1538-3873/aa65ba (2017). 1702.03653.

[16] Nikzad, S. et al. High-efficiency UV/optical/NIR detectors for large aperture telescopes and UV explorer missions: development of and field observations with delta-doped arrays. *Journal of Astronomical Telescopes, Instruments, and Systems* **3**, 036002, DOI: https://dx.doi.org/10.1117/1.JATIS.3.3.036002 (2017). 1612.04734.

[17] Wilson, J. C. et al. A Wide-Field Infrared Camera for the Palomar 200-inch Telescope. In Iye, M. & Moorwood, A. F. M. (eds.) Instrument Design and Performance for Optical/Infrared Ground-based Telescopes, vol. 4841 of Society of Photo-Optical Instrumentation Engineers (SPIE) Conference Series, 451–458, DOI: https://dx.doi.org/10.1117/12.460336 (2003).

[18] Aggarwal, K. et al. Probabilistic Association of Transients to their Hosts (PATH). *The Astrophysical Journal* **911**, 95, DOI: https://dx.doi.org/10.3847/1538-4357/abe8d2 (2021). 2102.10627.

[19] Oke, J. B. et al. The Keck Low-Resolution Imaging Spectrometer. *Publications of the ASP* **107**, 375, DOI: https://dx.doi.org/10.1086/133562 (1995).

[20] Faber, S. M. et al. The DEIMOS spectrograph for the Keck II Telescope: integration and testing. In Iye, M. & Moorwood, A. F. M. (eds.) Instrument Design and Performance for Optical/Infrared Ground-based Telescopes, vol. 4841 of Society of Photo-Optical Instrumentation Engineers (SPIE) Conference Series, 1657–1669, DOI: https://dx.doi.org/10.1117/12.460346 (2003).

[21] Oke, J. B. & Gunn, J. E. An Efficient Low Resolution and Moderate Resolution Spectrograph for the Hale Telescope. *Publications of the ASP* **94**, 586, DOI: https://dx.doi.org/10.1086/131027 (1982).

[22] Cappellari, M. Full spectrum fitting with photometry in PPXF: stellar population versus dynamical masses, non-parametric star formation history and metallicity for 3200 LEGA-C

galaxies at redshift z ≈ 0.8. *Monthly Notices of the Royal Astronomical Society* **526**, 3273–3300, DOI: https://dx.doi.org/10.1093/mnras/stad2597 (2023). 2208.14974.

[23] Johnson, B. D., Leja, J., Conroy, C. & Speagle, J. S. Stellar Population Inference with Prospector. *The Astrophysical Journal Supplement Series* **254**, 22, DOI: https://dx.doi.org/10.3847/1538-4365/abef67 (2021). 2012.01426.

[24] Dey, A. et al. Overview of the DESI Legacy Imaging Surveys. *The Astronomical Journal* **157**, 168, DOI: https://dx.doi.org/10.3847/1538-3881/ab089d10.48550/arXiv.1804.08657 (2019). 1804.08657.

[25] Alam, S. et al. The Eleventh and Twelfth Data Releases of the Sloan Digital Sky Survey: Final Data from SDSS-III. *The Astrophysical Journal Supplement Series* **219**, 12, DOI: https://dx.doi.org/10.1088/0067-0049/219/1/12 (2015). 1501.00963.

[26] Skrutskie, M. F. et al. The Two Micron All Sky Survey (2MASS). *The Astronomical Journal* **131**, 1163–1183, DOI: https://dx.doi.org/10.1086/498708 (2006).

[27] Cutri, R. M. et al. VizieR Online Data Catalog: AllWISE Data Release (Cutri+ 2013). *VizieR Online Data Catalog* II/328 (2021).

[28] Martin, D. C. et al. The Galaxy Evolution Explorer: A Space Ultraviolet Survey Mission. *The Astrophysical Journal Letters* **619**, L1–L6, DOI: https://dx.doi.org/10.1086/426387 (2005). astro-ph/0411302.

[29] Baldwin, J. A., Phillips, M. M. & Terlevich, R. Classification parameters for the emission-line spectra of extragalactic objects. *Publications of the ASP* **93**, 5–19, DOI: https://dx.doi.org/10.1086/130766 (1981).

[30] Kewley, L. J., Groves, B., Kauffmann, G. & Heckman, T. The host galaxies and classification of active galactic nuclei. *Monthly Notices of the Royal Astronomical Society* **372**, 961–976, DOI: https://dx.doi.org/10.1111/j.1365-2966.2006.10859.x (2006). astro-ph/0605681.

[31] Wright, E. L. et al. The Wide-field Infrared Survey Explorer (WISE): Mission Description and Initial On-orbit Performance. *The Astronomical Journal* **140**, 1868–1881, DOI: https://dx.doi.org/10.1088/0004-6256/140/6/1868 (2010). 1008.0031.

[32] Leja, J. et al. A New Census of the 0.2 < z < 3.0 Universe. I. The Stellar Mass Function. *The Astrophysical Journal* **893**, 111, DOI: https://dx.doi.org/10.3847/1538-4357/ab7e27 (2020). 1910.04168.

[33] Leja, J. et al. A New Census of the 0.2 < z < 3.0 Universe. II. The Star-forming Sequence. *The Astrophysical Journal* **936**, 165, DOI: https://dx.doi.org/10.3847/1538-4357/ac887d (2022). 2110.04314.

[34] Law, C. J. et al. Deep Synoptic Array Science: First FRB and Host Galaxy Catalog. *The Astrophysical Journal* **967**, 29, DOI: https://dx.doi.org/10.3847/1538-4357/ad3736 (2024). 2307.03344.

[35] Ocker, S. K., Cordes, J. M., Chatterjee, S. & Gorsuch, M. R. Radio Scattering Horizons for Galactic and Extragalactic Transients. *The Astrophysical Journal* **934**, 71, DOI: https://dx.doi.org/10.3847/1538-4357/ac75ba (2022). 2203.16716.

[36] Schulze, S. et al. The Palomar Transient Factory Core-collapse Supernova Host-galaxy Sample. I. Host-galaxy Distribution Functions and Environment Dependence of Core-collapse Supernovae. *The Astrophysical Journal Supplement Series* **255**, 29, DOI: https://dx.doi.org/10.3847/1538-4365/abff5e (2021). 2008.05988.

[37] Taggart, K. & Perley, D. A. Core-collapse, superluminous, and gamma-ray burst supernova host galaxy populations at low redshift: the importance of dwarf and starbursting galaxies. *Monthly Notices of the Royal Astronomical Society* **503**, 3931–3952, DOI: https://dx.doi.org/10.1093/mnras/stab174 (2021). 1911.09112.

[38] Heger, A., Fryer, C. L., Woosley, S. E., Langer, N. & Hartmann, D. H. How Massive Single Stars End Their Life. *The Astrophysical Journal* **591**, 288–300, DOI: https://dx.doi.org/10.1086/375341 (2003). astro-ph/0212469.

[39] Klencki, J., Nelemans, G., Istrate, A. G. & Pols, O. Massive donors in interacting binaries: effect of metallicity. *Astronomy and Astrophysics* **638**, A55, DOI: https://dx.doi.org/10.1051/0004-6361/202037694 (2020). 2004.00628.

[40] Sherman, M. B. et al. Searching for magnetar binaries disrupted by core-collapse supernovae. *Monthly Notices of the Royal Astronomical Society* **531**, 2379–2414, DOI: https://dx.doi.org/10.1093/mnras/stae1289 (2024). 2404.05135.

[41] Seebeck, J. et al. The Effects of Selection Biases on the Analysis of Localised Fast Radio Bursts. *arXiv e-prints* arXiv:2112.07639, DOI: https://dx.doi.org/10.48550/arXiv.2112.07639 (2021). 2112.07639.

[42] Bhardwaj, M. et al. A Nearby Repeating Fast Radio Burst in the Direction of M81. *The Astrophysical Journal Letters* **910**, L18, DOI: https://dx.doi.org/10.3847/2041-8213/abeaa6 (2021). 2103.01295.

[43] Kremer, K., Piro, A. L. & Li, D. Dynamical Formation Channels for Fast Radio Bursts in Globular Clusters. *The Astrophysical Journal Letters* **917**, L11, DOI: https://dx.doi.org/10.3847/2041-8213/ac13a010.48550/arXiv.2107.03394 (2021). 2107.03394.

[44] Sharma, K. et al. Deep Synoptic Array Science: A Massive Elliptical Host Among Two Galaxy-cluster Fast Radio Bursts. *The Astrophysical Journal* **950**, 175, DOI: https://dx.doi.org/10.3847/1538-4357/accf1d (2023). 2302.14782.

[45] Tauris, T. M., Sanyal, D., Yoon, S. C. & Langer, N. Evolution towards and beyond accretion-induced collapse of massive white dwarfs and formation of millisecond pulsars. *Astronomy and Astrophysics* **558**, A39, DOI: https://dx.doi.org/10.1051/0004-6361/201321662 (2013). 1308.4887.

[46] Ma, X. et al. The origin and evolution of the galaxy mass-metallicity relation. *Monthly Notices of the Royal Astronomical Society* **456**, 2140–2156, DOI: https://dx.doi.org/10.1093/mnras/stv2659 (2016). 1504.02097.

[47] Margalit, B. & Metzger, B. D. A Concordance Picture of FRB 121102 as a Flaring Magnetar Embedded in a Magnetized Ion-Electron Wind Nebula. *The Astrophysical Journal Letters* **868**, L4, DOI: https://dx.doi.org/10.3847/2041-8213/aaedad (2018). 1808.09969.

[48] Zhang, Z. J., Yan, K., Li, C. M., Zhang, G. Q. & Wang, F. Y. Intergalactic Medium Dispersion Measures of Fast Radio Bursts Estimated from IllustrisTNG Simulation and Their Cosmological Applications. *The Astrophysical Journal* **906**, 49, DOI: https://dx.doi.org/10.3847/1538-4357/abceb9 (2021). 2011.14494.

[49] Fong, W.-f. et al. Short GRB Host Galaxies. I. Photometric and Spectroscopic Catalogs, Host Associations, and Galactocentric Offsets. *The Astrophysical Journal* **940**, 56, DOI: https://dx.doi.org/10.3847/1538-4357/ac91d010.48550/arXiv.2206.01763 (2022). 2206.01763.